

Observation of oxygen pyramid tilting induced polarization rotation in strained BiFeO₃ thin film

Dongsheng Song^{1,2} | Heng-Jui Liu³ | András Kovács² | Rafal E. Dunin-Borkowski² | Ying-Hao Chu⁴ | Jing Zhu¹ 

¹National Center for Electron Microscopy in Beijing, Key Laboratory of Advanced Materials (MOE) and The State Key Laboratory of New Ceramics and Fine Processing, School of Materials Science and Engineering, Tsinghua University, Beijing, China

²Ernst Ruska-Centre for Microscopy and Spectroscopy with Electrons and Peter Grünberg Institute, Forschungszentrum Jülich, Jülich, Germany

³Department of Materials Science and Engineering, National Chung Hsing University, Taichung, Taiwan

⁴Department of Materials Science and Engineering, National Chiao Tung University, Hsinchu, Taiwan

Correspondence

Jing Zhu, National Center for Electron Microscopy in Beijing, Key Laboratory of Advanced Materials (MOE) and The State Key Laboratory of New Ceramics and Fine Processing, School of Materials Science and Engineering, Tsinghua University, Beijing 100084, China.
Email: jzhu@mail.tsinghua.edu.cn

Funding information

Chinese National Natural Science Foundation, Grant/Award Number: 51390471 and 51527803; National 973 Project of China, Grant/Award Number: 2015CB654902; National key research and development program, Grant/Award Number: 2016YFA0301001 and 2016YFB0700402; Chinese National Natural Science Foundation, Grant/Award Number: 51390471 and 51527803; European Research Council, Grant/Award Number: FP7, 2007-2013 and 320832; Seventh Framework Programme; Tsinghua University

Abstract

Oxygen octahedral tilting has been recognized to strongly interact with spin, charge, orbital, and lattice degrees of freedom in perovskite oxides. Here, we observe a strain-driven stripe-like morphology of two supertetragonal (monoclinic *Cc* and *Cm*) phases in the strained BiFeO₃/LaAlO₃ thin films. The two supertetragonal phases have a similar giant axial ratio but differences in oxygen pyramid tilting mode. Especially, the competition between polar instability and oxygen pyramid tilting is identified using atomically resolved scanning transmission electron microscopy, leading to the polarization rotation across the phase boundary. In addition, microtwins are observed in the *Cc* phase. Our findings provide new insights of the coupling between ferroelectric polarization and oxygen pyramid tilting in oxide thin films and will help to design novel phase morphology with desirable ferroelectric polarization and properties for new applications in perovskite oxides.

KEYWORDS

ferroelectricity/ferroelectric materials, multiferroics, perovskites, polarization, thin films

1 | INTRODUCTION

The oxygen octahedral tilting, which is usually defined as the configuration of the corner-connective— BO_6 —octahedra in perovskite oxides (ABO_3), has been recognized to strongly interact with these degrees of freedom (spin, charge, orbital, and lattice)^{1–3} and affect the macroscopic electrical/magnetic properties.^{4–14} Among them, the interplay between ferroelectric polar order and octahedra tilting has been theoretically⁴ and experimentally^{5,13} studied in the ABO_3 thin films, such as the ferroelectricity at the interface between nonpolar ABO_3 oxides,^{4,15,16} polarization rotation in PbTiO_3 thin films,¹³ suppression of polarization in the BiFeO_3 (BFO) thin films.⁵ Moreover, the manipulation of polarization by oxygen octahedra tilting could further affect their ferroelectric or piezoelectric response to external electrical field, demonstrating an extraordinary opportunity to control the multifunctional properties in ABO_3 oxides.

Different oxygen octahedral tilting modes will modify the polarization in different ways.^{5,13} The ABO_3 oxides thin films are always exhibited with plenty of phase structures with different oxygen octahedral tilting modes stabilized by epitaxial strain. Therefore, it is expected to observe the coexistence of different octahedral tilting modes with different resultant polarization modulation in the strained ABO_3 thin films. BFO is a very promising prototype,^{17–20} which has the phase transition that follows the sequence $R\text{-}M_A(\text{R-like})\text{-}M_C(\text{T-like})\text{-}T$ phases^{21–24} with the increasing

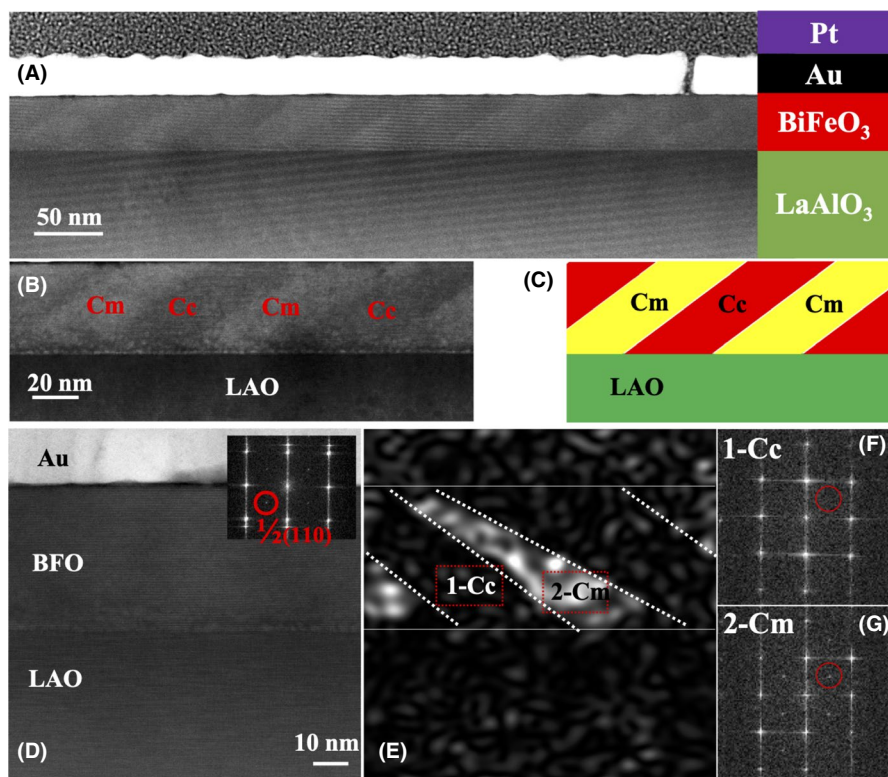
epitaxial strain. The accurately structural determination of BFO has inferred that the *T-like* phase crystallizes in two different space groups, which correspond to *Cc* and *Cm* monoclinic phases that exhibit either an out-of-phase mode (R_4^+) of the oxygen pyramids in two directions or an in-phase mode (M_3^+) in one direction, respectively.^{25,26} Their different oxygen pyramid tilting modes might contribute to the polarization rotation as predicted by first-principles calculations.²⁷

Here, polarization rotation induced by oxygen pyramid tilting is directly observed by atomic resolution aberration corrected scanning transmission electron microscopy (STEM) in the BFO/ LaAlO_3 (LAO) thin films with an intermediate thickness of 40 nm. Two strain-driven stripe-like supertetragonal phases (monoclinic *Cm* and *Cc*), both with a large tetragonality, exhibit obvious polarization rotation across the phase boundary induced by different oxygen pyramid tilting modes. Moreover, microtwins in the *Cc* phase with large in-plane polarization are observed, which was not previously observed by X-ray or other macro-structural measurements.

2 | EXPERIMENTAL RESULTS AND DISCUSSION

40 nm and 57 nm BFO thin films were epitaxially grown on (001)-oriented LAO single crystal substrates using pulsed laser deposition (PLD). Figure 1A shows a low magnification high-angle annular dark-field STEM (HAADF-STEM) image of a

FIGURE 1 Stripe-like tetragonal phases in BFO/LAO films of thickness 40 nm. A, Low magnification HAADF-STEM image. B, Enlarged image and schematic diagram show the stripe-like phases. C, Schematic diagram of stripe-like phases. D, High-resolution HAADF-STEM image with FFT inset. A red circle marks a $\frac{1}{2}(110)$ extra spot. E, DDF images generated from the extra spots in (D). F, G, FFTs of the *Cc* and *Cm* phases, respectively. All the images are taken under the [100] zone axis [Color figure can be viewed at wileyonlinelibrary.com]



40 nm BFO film. Stripe-like bright and dark contrast is clearly observed, as shown in the enlarged image in Figure 1B. It should be noted that the stripe-like contrast can be distinguished from that produced by *R-like* and *T-like* phases, which appears in films of greater thickness,²⁰ such as the 57 nm BFO thin film in Figure S1. In order to further understand the atomic structures of the two phases, high-resolution HAADF-STEM images were recorded in Figure 1D. A fast Fourier Transform (FFT) is displayed in the inset. The spots in the FFT are split along the *c* direction because of the large lattice mismatch between LAO and BFO. The *c/a* ratio is estimated to be ~ 1.23 , as a result of the larger tetragonality of the *T-like* phase. After carefully examining FFTs from different localized areas, two *T-like* phases are found in Figure 1F,G. The primary difference is the presence of extra $\frac{1}{2}(110)$ superreflection spots. The generation of a digital dark-field (DDF) image from the extra spots base on the STEM images reveals two *T-like* phases in Figure 1E.

As the rich phase structures of BFO have already been widely studied before, our results here should be also within the realm of these possibilities. By comparing the two *T-like* phases

with previous experimental and theoretical results and carefully examining these structure models in the literatures,^{25,26,28} it can be inferred that they are monoclinic *Cc* or *Cm* phases with the atomic model in Figure 2A,D, respectively. Although some other possibilities might exist, the explanations here might be the most reasonable one. More detailed analysis can be found in Figure S2. The phase with the extra $\frac{1}{2}(110)$ spots corresponds to the *Cm* phase, with an in-phase mode (M_3^+) of oxygen pyramid tilting in one direction that doubles the unit cell of BFO. Figure 2B shows the simulated diffraction pattern of *Cm* phase along the [100] direction, consistent with the FFT analysis above and the nanodiffraction result in Figure 2C. The oxygen pyramid is ordered along the [110] direction, as indicated by a red dotted line in Figure 2A, with the oxygen pyramid tilting alternately toward the left or right. Note that the *Cm* phase here is the same as the *T-like* phase in the 57 nm BFO film in Figure S1, consistent with previous reports^{28,29}. The phase without the extra $\frac{1}{2}(110)$ spots is the *Cc* phase, which always exists in ultrathin BFO films on LAO.^{26,28} The stripe-like morphology with two *T-like* phases, rather than a mixture of *T-like* and *R-like* phases,

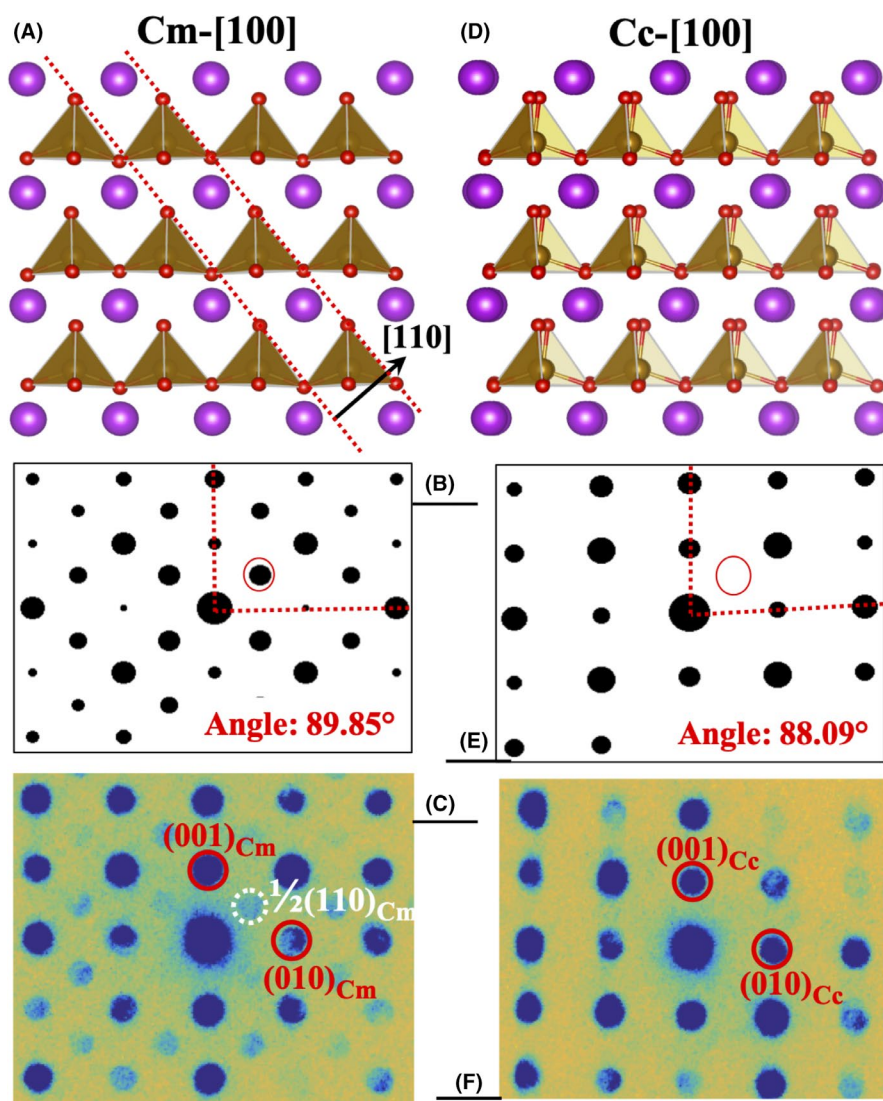


FIGURE 2 Atomic model and electron diffraction patterns for the *Cm* and *Cc* phases. A, D, Atomic models of the *Cm* and *Cc* phases, respectively, viewed along the [100] direction. The red dotted lines mark (110) planes with ordered oxygen pyramid tilting. B, E, Simulated electron diffraction patterns corresponding to the structural models in (A) and (B) along [100] direction, respectively. C, F, Electron nanodiffraction patterns of *Cm* and *Cc* phases, respectively [Color figure can be viewed at wileyonlinelibrary.com]

is observed at intermediate thicknesses of BFO on LAO. Additionally, the *Cc* and *Cm* phases show almost no obvious difference in chemical composition as discussed in Figure S4.

Geometrical phase analysis (GPA)³⁰ was further used to map the strain fields in the thin films. Figure 3A,C show experimental maps of in-plane (e_{xx}) and out-of-plane (e_{yy}) deformation, respectively. The stripe-like contrast is clear in the in-plane deformation map because of the different in-plane lattice parameters a . However, the deformation e_{xx} is very small, as indicated by the line profile in Figure 3B. The difference in out-of-plane deformation between the *Cm* and *Cc* phases is negligible. Maps of the lattice parameters a , c , and c/a determined from accurately measured atomic positions are shown in Figure 3D-F. These results are consistent with the GPA analysis, with $a_{\text{LAO}} \approx a_{C_c} > a_{C_m}$ and $c_{C_m} \approx c_{C_c} > c_{\text{LAO}}$. The large tetragonality of ~ 1.23 and 1.21 are respectively observed for *Cm* and *Cc* phases in Figure 3G, with a transition region of approximately 3-4 unit cells at both interfaces, indicating a relaxation of the lattice in the growth direction away from the interface.³¹ The variation of the in-plane lattice parameter a is shown in Figure 3H. For the *Cc* phase, it is uniform throughout the film. While for the *Cm* phase, it has a constant value only for the first 5-6 unit cells, after which it gradually decreases by ~ 5 PM. Therefore, very small difference in lattice parameters and strain is existing between the *Cc* and *Cm* phases, except for the different oxygen pyramid tilting modes.

In BFO, the lattice is strongly coupled to the polarization. Different oxygen pyramid tilting modes could lead to different ferroelectric properties of the *Cm* and *Cc* phases. Figure 4A shows unit cell by unit cell polarization mapping across a phase

boundary. The polarization is defined as the displacement of Fe atom columns with respect to the center of four nearest Bi atom columns surrounding it. Figure 4B shows a corresponding HAADF-STEM image with an overlaid map of the lattice parameter a , on which the *Cm* and *Cc* phases can be identified. The polarization direction rotates from $\sim 87^\circ$ in the *Cm* phase to $\sim 64^\circ$ in the *Cc* phase, as indicated in Figure 4C. The *Cm* phase has a giant out-of-plane and a small in-plane polarization, resulting in a tetragonal-like polarization. In the *Cc* phase, the in-plane polarization is very high. Although the monoclinic distortions of the *Cc* phase could explain why the polarization is not aligned strictly along [001] direction,²⁸ it cannot contribute to such a large polarization rotation in the highly tetragonal *Cc* phase. Apart from the very small difference in lattice parameter a , the different oxygen pyramid tilting modes should be the primary origin of the differently polarized states. The *Cc* phase with a large in-plane polarization is further confirmed by analyzing different areas in Figure S3 in the stripe-like phases. Note that the tilting angle of the polarization in the *Cc* phase in Figure S3 does not always have a single value, indicating that there is a different degree of competition in different parts of the film, which might be caused by the varied proportion of microtwins in the *Cc* phase discussed below. Previous theoretical calculations have revealed the important role of oxygen octahedra tilting, which opposes any natural enhancement of the out-of-plane polarization.²⁷ The antiferrodistortive rotation of oxygen pyramids with an in-phase (R_4^+) mode and polar instabilities of the *Cc* phase compete with each other and contribute to a ground state that has a large in-plane polarization. The value of polarization remains almost the same for the *Cc* and *Cm* phases, as shown in Figure 4D, in contrast to previous

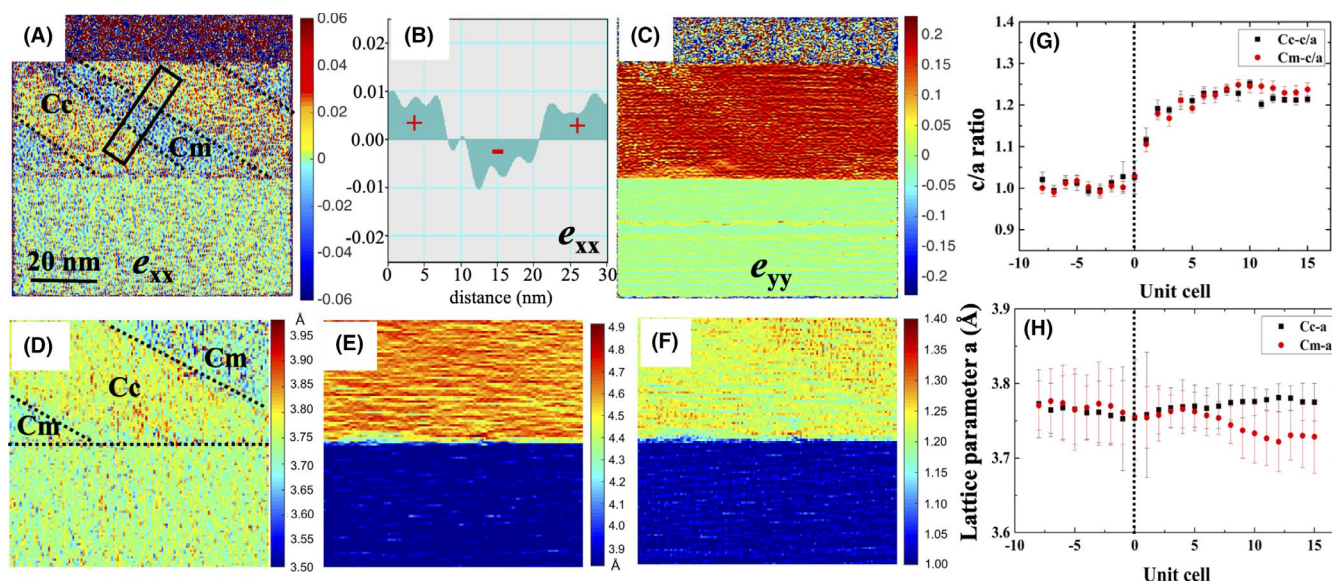


FIGURE 3 Mapping of strain field and lattice parameters of the stripe-like phases under the [100] zone axis. A, C, In-plane (e_{xx}) and out-of-plane (e_{yy}) deformation, respectively, measured using GPA. B, Line profile obtained from the rectangle in (A), illustrating the deformation across the phase boundary. D-F, Lattice parameters a , c and c/a , respectively. Lattice parameters c/a (G) and a (H) of *Cc* and *Cm* phases measured as a function of distance from the interface in BFO/LAO (40 nm) thin films [Color figure can be viewed at wileyonlinelibrary.com]

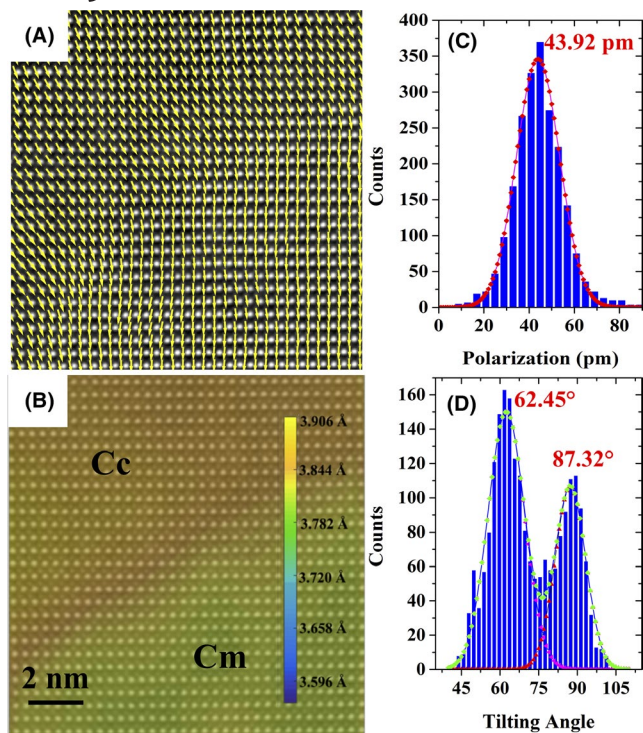


FIGURE 4 Polarization mapping of the *Cc* and *Cm* phases under [100] zone axis. A, Mapping of polarization across a phase boundary. B, Mapping of lattice parameter *a* superimposed onto an HRSTEM image. C, D, Histograms of polarization and tilt angle from (A), respectively [Color figure can be viewed at wileyonlinelibrary.com]

calculations²⁷ stating that the *Cc* phase has a lower total amplitude of polarization with a similar misfit when compared with the *Cm* phase. The *c/a* value for the *Cc* phase (~ 1.21) is much larger than the theoretical prediction (~ 1.15)²⁷ and not observed before. Our results provide the experimental evidence of a competition between oxygen pyramid tilting and out-of-plane polarization in the stripe-like morphology of the BFO films.

As the *Cc* phase with a large in-plane polarization and tetragonality has not been predicted by theoretical calculation, it might be a metastable phase observed here in the strained BFO thin films. The further detailed analysis reveals the microtwins in the *Cc* phase as shown in Figure 5A, 5, which are absent in the *Cm* phase. The microtwins are resolved by giving the rotation angle of atomic planes in the grown direction, which was calculated by the GPA script developed by Christoph T. Koch. We attribute these microtwins to the 180° in-plane rotations in the *Cc* phase along the [100] or $[-100]$ directions. The corresponding atomic model is shown in Figure 5C. The rotation angle of $\sim 3.8^\circ$ in the model is consistent with the experimental rotation map shown in Figure 5A. The existence of microtwins can partially accommodate the internal strain and stabilize the metastable *Cc* phase. Obviously, the microtwins are not homogeneous in the *Cc* phase as shown in Figure 5A, which might contribute to the varied tilting angle of polarization as discussed above.

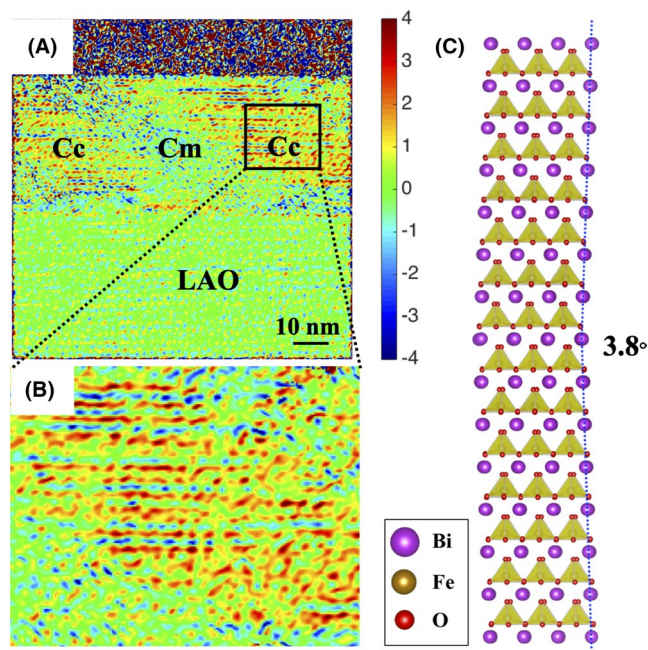


FIGURE 5 Microtwins in the *Cc* phases under the [100] zone axis. A, Rotation map of the *Cc* and *Cm* stripe-like phases in the growth direction. The units in the color bar are degrees. B, Enlarged area shows microtwins in the *Cc* phase in the marked region in (A). C, Atomic model of an in-plane 180° rotation in the *Cc* phase [Color figure can be viewed at wileyonlinelibrary.com]

Based on the above structural and strain analysis of the BFO/LAO thin films, we attribute the formation of these phase structures observed here to the appropriate strain at an intermediate thickness. For very thin BFO film, such as 7 nm as reported before²⁶, the *Cc* phase is stabilized in the whole thin films without any microtwins. For the thick BFO film, such as 57 nm here, the *Cm* and *R* phases are coexisting. Therefore, the transition from *Cc* to *Cm* phase will occur with the increasing film thickness. We speculate the phase evolution as follows. Firstly, the *Cc* phase is stabilized in the very thin BFO films but the microtwins are absent owing to the fully strain state. Then, with the increasing thickness, partial strain will be gradually relaxed through forming the microtwins in the *Cc* phase. Furthermore, some regions of *Cc* phase will transform into the *Cm* phase with the increasing strain relaxation. Consequently, the stripe-like phase morphology of *Cm* and *Cc* phases are formed.

3 | CONCLUSION

In summary, the nanoscale strain-driven stripe-like supertetragonal phases are observed in a BFO/LAO thin film of intermediate thickness. Stripes are formed of *Cc* and *Cm* phases, with a large tetragonality and different oxygen pyramid tilting modes. The competition between oxygen pyramid tilting and out-of-plane polarization is

directly observed, leading to the polarization rotation in the *Cc* phase. Microtwins in the *Cc* phase are identified to release the strain of the metastable phase. Our results demonstrate the direct experimental evidence of the interplay between polarization rotation and oxygen pyramid tilting in the strained BiFeO₃ thin films, which might be used to design desirable ferroelectric polarization and properties in perovskite oxides.

ACKNOWLEDGMENTS

This work was financially supported by Chinese National Natural Science Foundation (51788104, 51390471, 51527803, 51761135131), National 973 Project of China (2015CB654902), and National key research and development program (2016YFB0700402 and 2016YFA0301001). This work made use of the resources of the National Center for Electron Microscopy in Beijing and the Ernst Ruska-Centre for Microscopy and Spectroscopy with Electrons in Jülich. The research leading to these results received funding from the European Research Council under the European Union's Seventh Framework Programme (FP7/2007-2013)/ERC grant agreement number 320832. DS acknowledges a Scholarship for Overseas Graduate Studies at Tsinghua University.

ORCID

Jing Zhu  <https://orcid.org/0000-0002-2175-9476>

REFERENCES

- Wang KF, Liu J-M, Ren ZF. Multiferroicity: the coupling between magnetic and polarization orders. *Adv Phys.* 2009;58(4):321–448.
- Hwang HY, Iwasa Y, Kawasaki M, Keimer B, Nagaosa N, Tokura Y. Emergent phenomena at oxide interfaces. *Nat Mater.* 2012;11(2):103–13.
- Chakhalian J, Freeland JW, Millis AJ, Panagopoulos C, Rondinelli JM. Colloquium: emergent properties in plane view: Strong correlations at oxide interfaces. *Rev Mod Phys.* 2014;86(4):1189–202.
- Rondinelli JM, Fennie CJ. Octahedral rotation-induced ferroelectricity in cation ordered perovskites. *Adv Mater.* 2012;24(15):1961–8.
- Kim Y-M, Kumar A, Hatt A, Morozovska AN, Tselev A, Biegalski MD, et al. Interplay of octahedral tilts and polar order in BiFeO₃ Films. *Adv Mater.* 2013;25(17):2497–504.
- Hatt AJ, Spaldin NA. Structural phases of strained LaAlO₃ driven by octahedral tilt instabilities. *Phys Rev B.* 2010;82(19):195402.
- Sim H, Cheong SW, Kim BG. Octahedral tilting-induced ferroelectricity in ASnO₃/BSnO₃ superlattices. *Phys Rev B.* 2013;88(1):014101.
- Borisevich AY, Chang HJ, Huijben M, Oxley MP, Okamoto S, Niranjana MK, et al. Suppression of octahedral tilts and associated changes in electronic properties at epitaxial oxide heterostructure interfaces. *Phys Rev Lett.* 2010;105(8):087204.
- Levin I, Krayzman V, Cibin G, Tucker MG, Eremenko M, Chapman K, et al. Coupling of emergent octahedral rotations to polarization in (K, Na)NbO₃ ferroelectrics. *Sci Rep.* 2017;7(1):15620.
- He J, Borisevich A, Kalinin SV, Pinnycok SJ, Pantelides ST. Control of octahedral tilts and magnetic properties of perovskite oxide heterostructures by substrate symmetry. *Phys Rev Lett.* 2010;105(22):227203.
- Liao Z, Huijben M, Zhong Z, Gauquelin N, Macke S, Green RJ, et al. Controlled lateral anisotropy in correlated manganite heterostructures by interface-engineered oxygen octahedral coupling. *Nat Mater.* 2016;15(4):425–31.
- Kan D, Aso R, Sato R, Haruta M, Kurata H, Shimakawa Y. Tuning magnetic anisotropy by interfacially engineering the oxygen coordination environment in a transition metal oxide. *Nat Mater.* 2016;15(4):432–7.
- Zhang S, Guo X, Tang Y, Ma D, Zhu Y, Wang Y, et al. Polarization rotation in ultrathin ferroelectrics tailored by interfacial oxygen octahedral coupling. *ACS Nano.* 2018;12(4):3681–8.
- Rondinelli JM, Spaldin NA. Substrate coherency driven octahedral rotations in perovskite oxide films. *Phys Rev B.* 2010;82(11):113402.
- Benedek N, Rondinelli J, Djani H, Ghosez P, Lightfoot P. Understanding ferroelectricity in layered perovskites: new ideas and insights from theory and experiments. *Dalton Trans.* 2015;44(23):10543–58.
- Young J, Rondinelli JM. Atomic scale design of polar perovskite oxides without second-order Jahn-Teller ions. *Chem Mater.* 2013;25(22):4545–50.
- Catalan G, Scott JF. Physics and applications of bismuth ferrite. *Adv Mater.* 2009;21(24):2463–85.
- Schlom DG, Chen L-Q, Eom C-B, Rabe KM, Streiffer SK, Triscone J-M. Strain tuning of ferroelectric thin films. *Annu Rev Mater Res.* 2007;37(1):589–626.
- Yang J-C, He Q, Yu P, Chu Y-H. BiFeO₃ thin films: a playground for exploring electric-field control of multifunctionalities. *Annu Rev Mater Res.* 2015;45(1):249–75.
- Zeche RJ, Rossell MD, Zhang JX, Hatt AJ, He Q, Yang C-H, et al. A strain-driven morphotropic phase boundary in BiFeO₃. *Science.* 2009;326(5955):977.
- Chen Z, Luo Z, Huang C, Qi Y, Yang P, You LU, et al. Low-symmetry monoclinic phases and polarization rotation path mediated by epitaxial strain in multiferroic BiFeO₃ thin films. *Adv Func Mater.* 2011;21(1):133–8.
- Zhang JX, Xiang B, He Q, Seidel J, Zeche RJ, Yu P, et al. Large field-induced strains in a lead-free piezoelectric material. *Nat Nanotechnol.* 2011;6(2):98–102.
- Beekman C, Siemons W, Ward TZ, Chi M, Howe J, Biegalski MD, et al. Phase transitions, phase coexistence, and piezoelectric switching behavior in highly strained BiFeO₃ films. *Adv Mater.* 2013;25(39):5561–7.
- Christen HM, Nam JH, Kim HS, Hatt AJ, Spaldin NA. Stress-induced R – MA – MC – T symmetry changes in BiFeO₃ films. *Phys Rev B.* 2011;83(14):144107.
- Diéguez O, González-Vázquez OE, Wojdeł JC, Íñiguez J. First-principles predictions of low-energy phases of multiferroic BiFeO₃. *Phys Rev B.* 2011;83(9):094105.
- Pailloux F, Couillard M, Fusil S, Bruno F, Saidi W, Garcia V, et al. Atomic structure and microstructures of supertetragonal multiferroic BiFeO₃ thin films. *Phys Rev B.* 2014;89(10):104106.
- Dupé B, Infante IC, Geneste G, Janolin PE, Bibes M, Barthélémy A, et al. Competing phases in BiFeO₃ thin films under compressive epitaxial strain. *Phys Rev B.* 2010;81(14):144128.

28. Béa H, Dupé B, Fusil S, Mattana R, Jacquet E, Warot-Fonrose B, et al. Evidence for room-temperature multiferroicity in a compound with a giant axial ratio. *Phys Rev Lett.* 2009;102(21):217603.
29. Rossell MD, Erni R, Prange MP, Idrobo JC, Luo W, Zeches RJ, et al. Atomic Structure of Highly Strained BiFeO₃ Thin Films. *Phys Rev Lett.* 2012;108(4):047601.
30. Hÿtch MJ, Snoeck E, Kilaas R. Quantitative measurement of displacement and strain fields from HREM micrographs. *Ultramicroscopy.* 1998;74(3):131–46.
31. Huang R, Ding H-C, Liang W-I, Gao Y-C, Tang X-D, He Q, et al. Atomic-scale visualization of polarization pinning and relaxation at coherent BiFeO₃/LaAlO₃ interfaces. *Adv Func Mater.* 2014;24(6):793–9.

SUPPORTING INFORMATION

Additional supporting information may be found online in the Supporting Information section.

Supinfo

How to cite this article: Song D, Liu H-J, Kovács A, Dunin-Borkowski RE, Chu Y-H, Zhu J. Observation of oxygen pyramid tilting induced polarization rotation in strained BiFeO₃ thin film. *J Am Ceram Soc.* 2020;103:2828–2834. <https://doi.org/10.1111/jace.16937>